https://doi.org/10.1016/j.jlumin.2016.12.024

Excitation energy transfer in Ruthenium (II)-porphyrin conjugates led to enhanced emission quantum yield and $^1O_2$ generation

Jie Pan,[a] Lijun Jiang, [a] Chi-Fai Chan, [a] Tik-Hung Tsoi, [b] Kwok-Keung, Shiu,*[a] Daniel W. J. Kwong, *[a] Wing-Tak Wong, *[b] Wai-Kwok Wong, *[a] and Ka-Leung Wong*[a]

[a] Department of Chemistry, Hong Kong Baptist University. Kowloon Tong, Hong Kong SAR
[b] Department of Applied Biology and Chemical Technology, Hung Hom, Hong Kong SAR
*Corresponding author. E-mail address: wkwong@hkbu.edu.hk, klwong@hkbu.edu.hk

Abstract:

Porphyrins are good photodynamic therapy (PDT) agents due to its flexibility for modifications to achieve tumor localization and photo-cytotoxicity against cancer. But their applications are hindered by poor water-solubility and low cell-permeability. It was found that, in a Ru(polypyridyl)-porphyrin system, the Ru(polypyridyl) and porphyin have similar excited state energies; a small perturbation (e.g. Zn(II) metalation) would lead to a marked change in the energy migration process. In this work, we have synthesized a series of porphyrins conjugated with Ru(polypyridyl) complexes using different linkers and investigated their photophysical properties, which included singlet oxygen quantum yield and their *in vitro* biological properties, resulting from linker variation and porphyrin modification by Zn(II) metalation.

Keywords: Luminescent material, Fluorescence probe, Porphyrin, Photodynamic therapy, Ruthenium.

1. Introduction

Porphyrins and its analogues have been used as photosensitizers in anti-cancer photodynamic therapy (PDT) owing to their preferential accumulation in tumour cells, i.e., ca. 2- to 5-fold higher than that in normal cells and their ability to induce oxidative damage to various vital cellular components, such as DNA, proteins and membrane components, thus causing cell death. [1-4] Most of the clinically approved porphyrin-based PDT agents absorb light mostly at their Q-bands, i.e. at *ca.* 600 nm where tissue penetration is better, rather than at the strongly-absorbing but not tissue- transparent Soret bands (*ca.* 430 nm) of the porphyrin moiety. However, this difficulty can be circumvented by the simultaneous absorption of two near-infrared photons at *ca.* 860 nm by the Soret bands to produce two-photon excited luminescence for imaging and $^1O_2$ for PDT. Excitation at 860 nm can offer deep tissue penetration and also has no "heating" effect on the water molecules compared to typical upconversion materials for imaging and PDT. [5] In the literature, most porphyrins do not exhibit a strong two-photon absorption cross-section, but it can be significantly enhanced by conjugation with ruthenium(II)-polypyridyl complex for effective PDT. [6] Incidentally, Ru(II)-polypyridine complexes have been shown to cause potent damage to tumour cells through their intercalation into double-stranded DNA and RNA, thus interfering with the strand separation during cell division. [7-9] In fact, some ruthenium complexes have recently been developed as anti-cancer PDT agents as

well. [10,11] In our earlier study, we examined the effect of linker on the properties of porphyrin-ruthenium conjugates. [12] The conjugate with a rigid linker has been shown to have the most promising *in vitro* photobiological properties for further development as a bifunctional probe for two-photon (NIR) induced PDT and tumour imaging. With the objective to design novel three-component (i.e., porphyrin-linker- Ru(II) complex) supra-molecular systems for tumour imaging and PDT applications,it is important that the excitation energy transfer mechanism between these components be elucidated, particularly when the excited-state energies of the porphyrin and the Ru-polypyridine moieties are very close. Different substituentgroups on the porphyrin and the choice of linkers can potentially exert significant effects on the water solubility, cellular uptake, subcellular localization, and, more importantly, the direction and efficiency of excitation energy transfer in these conjugates. A comprehensive evaluation of the luminescence quantum yields and PDTefficacies will furnish important data for an understanding of the energy transfer mechanism and for achieving an optimised design for PDT and tumour imaging applications of these conjugates.

In fact, controlled manipulation of the energy flow in photo-/redox-active supramolecular systems is crucial to diverse research fields, ranging from artificial photosynthesis, photocatalysis to photovoltaics. [13-15] Many parameters, such as light, redox potential, solvent used, pH, the effects of co-existing ligand and nearby ions have been found to play a role. [16-17] Recently, Tsuge and coworkers have found that energy transfer in porphyrin-Ru conjugates takes place from the Ru(II)

^{3}MLCT state to the porphyrin singlet state; but an introduction of Zn(II) ion into the porphyrin can increase its excited-state energy level, resulting in a reversal of the direction of energy transfer. [18,19]

In this work, two water-soluble free-base porphyrin-Ru(II) conjugates, **1**-**2**, and two Zn(II) porphyrin-Ru(II) conjugates, **3**-**4**, with flexible non-π-conjugative and rigid π-conjugative linkers incorporated between the hydrophobic porphyrin moiety and the hydrophilic Ru(II)-polypyridyl complex have been synthesized. The energy transfer mechanism in these porphyrin-ruthenium conjugates has been discussed. The introduction of Zn(II) into the porphyrin was shown to re-direct the excitation energy flow compared to their free-base counterparts by a comprehensive studies of their UV-Vis absorption and emission spectra. Their $^1O_2$ and emission quantum yields were measured and compared, which show that the free-base porphyrin-Ru(II) conjugates, **1**-**2**, affords a higher $^1O_2$ quantum yield, relative to the two Zn(II) porphyrin-Ru(II) conjugates, **3**-**4**. In *in vitro* studies, **1** and **2** shown stronger PDT activities than **3**-**4**, presumably due to their higher singlet oxygen quantum yields.

2. Experimental Sections

2.1 General information for syntheses.

All the chemicals were purchased commercially and used without further purification. All analytical grade solvents were dried by standard procedures. All the reactions were performed under nitrogen atmosphere, unless otherwise noted. Merck silica gel (60, particle size 0.040 - 0.063 mm) was used for flash column

chromatography. NMR spectra were recorded on Brüker Advance 400 (1H: 400 MHz). The following abbreviations were used to explain the multiplicities: s = singlet,d = doublet, t = triplet, q = quartet, m = multiplet. High-resolution mass spectra were obtained from Applied Biosystems (ABI) Q-Star Elite MALDI-TOF mass spectrometer. The synthetic routes for all compounds were described in the supportinginformation

Synthesis of of 2-bromo-N-(1,10-phenanthrolin-5-yl)acetamide

5-amine-1, 10-phenanthroline (600 mg, 3.076 mmol) and 0.3 mL 2-bromoaacetyl bromide was added in 100 mL chloroform refluxed overnight. Once the reaction completed, cooled the solution to room temperature, the solution was filtered through Buckner funnel, the precipitant was washed by methanol several times, the yellow solid was yield 550 mg, 56.8%.

Synthesis of 5,10,15-Tris(3',4',5'-trimethoxylphenyl)-20-(4'-hydoxyl-phenyl)-21H,23H-porphyrin (Por-OH)

3,4,5-trimethoxylbenzaldehyde (10.0 g, 0.051 mol) and 4-hydroxylbenzaldehyde (2.14 g, 0.0175 mol) was added in 300 mL of propionic acid, the temperature was raised to 140 °C, and then a solution of pyrrole (4.4 g, 0.0656 mol) in 50 mL propionic acid was added dropwise. Then the solution was refluxed for 3 h. When the reaction is finished, the propionic acid was distilled off under reduced pressure. The remaining solid was purified by column chromatography ($CHCl_3$ as eluent). The

purple product was yield 3.3 g, 20%. ^{1}H NMR ($CDCl_3$) δ -2.81 (s, 2H), 3.95 (s, 18H), 4.16 (s, 9H), 5.30 (s, 1H), 7.22 (m, 2H), 7.45 (s, 6H), 8.05 (d, 2H, *J* = 8.4Hz), 8.87 (d, 2H, *J* = 8.4 Hz), 8.92 (d, 6H, *J* = 4.8 Hz). HRMS (MALDI-TOF): Calcd. for $C_{53}H_{48}N_4O_{10}$, 900.9; Found for $[M+H]^+$, 901.3.

Synthesis of Amide-Linked Porphyrin-Phen (L1).

2-Bromo-N-(1,10-phenanthrolin-5-yl) acetamide (50 mg, 0.159 mmol) and excess amount of Cs_2CO_3 were added into a solution of **Por-OH** (50 mg, 0.056 mmol) in anhydrous DMF were stirred for 24 h at 80 °C. Organic phase was extracted by $CHCl_3$, and get rid of aqueous phase. The residue was purified on silica gel witheluent $CHCl_3$/MeOH (v/v = 30:1). Yield 25 mg, 40%. ^{1}H NMR ($CDCl_3$) δ -2.76 (s, 2H), 3.97 (s, 18H), 4.19 (s, 9H), 5.12 (s, 2H), 7.07-7.11 (m, 6H), 7.12 (d, 2H, *J* = 8.2 Hz), 7.69-7.72 (m, 1H), 7.80- 7.84 (m, 1H), 8.27 (d, 2H, *J* = 8.4 Hz), 8.33-8.35 (dd, 1H, *J* = 1.6 Hz, 8.1 Hz), 8.44-8.46 (dd, 1H, *J* = 1.5 Hz, 8.4 Hz), 8.57 (s, 1H), 8.88 (d, 2H, *J* = 4.7 Hz), 8.98 (s, 6H), 9.14 (s, 1H), 9.20-9.22(dd, 1H, *J* = 1.7Hz, 4.4Hz), 9.32 (dd, 1H, *J* = 1.7Hz, 4.1Hz). HRMS (MALDI-TOF) ($[M]_+$): Calcd. for $C_{67}H_{57}N_7O_{11}$, 1136.2; Found for $[M]^+$, 1136.4567.

Synthesis of Amide-Linked [(Porphyrin-Phen)Ru(bpy)$_2$][Cl]$_2$ (1)

L1(20 mg, 17.6 mmol) and *cis*-$Ru(bpy)_2Cl_2$ (34.1 mg, 105.6 mmol) was dissolved in the mixture of THF (15 mL) and ethanol (15 mL) solution. The solution was refluxed overnight. The solvent was removed under reduced pressure. The crude residue was

purified on neutral Al_2O_3 for column chromatography with eluent $CHCl_3$/MeOH (v/v = 20:1). Yield 20 mg, 66%. ^{1}H NMR (DMSO-d_6) δ -2.90 (s, 2H), 3,91 (s, 18H), 4.01 (s, 9H), 5.12 (s, 2H), 7.38-7.43 (m, 2H), 7.52-7.61 (m, 8H), 7.61-7.63 (m, 4H), 7.86-7.90 (m, 3H), 7.99 (dd, 1H, *J* = 8.8, 8.4Hz), 8.08-8.17 (m, 2H), 8.18- 8.26 (m, 6H), 8.81 (s, 1H), 8.85-8.94 (m, 7H), 8.97 (s, 6H), 9.21 (d, 1H, *J* = 8.8Hz), 11.38 (s, 1H). HRMS (MALDI-TOF) ([M-2Cl]$^+$, m/z): Cald. for $C_{87}H_{73}N_{11}O_{11}Ru$, 1549.45; Found for [M-2Cl]$^+$, 1549.4567.

Synthesis of Amide-Linked [(Zinc Porphyrin-Phen)Ru(bpy)$_2$][Cl]$_2$ (3)

Conjugates **1** (20 mg, 0.013 mmol) and excess amount of $Zn(OAc)_2.2H_2O$ (20 mg, 0.124 mmol) were dissolved in the mixture of THF (15 mL) and ethanol (15 mL) solution. After refluxed for 2 h, the solvent was removed under reduced pressure. Purified the residue on neutral Al_2O_3 with eluent $CHCl_3$/MeOH (v/v = 20:1). Yield 30 mg, 76%. ^{1}H NMR (DMSO-d_6) δ 3.91 (s, 18H), 4.01 (s, 9H), 7.48-7.49 (m, 5H), 7.50-7.57 (m, 4H), 7.60-7.69 (m, 5H), 7.74-7.77 (d, 4H, *J* = 5.2 Hz), 7.82-7.97 (m, 2H), 8.10-8.18 (m, 2H), 8.18-8.28 (m, 6H), 8.81-8.85 (m, 2H), 8.89-8.94 (m, 13H), 9.31-9.40 (d, 1H, *J* = 8Hz). HRMS (MALDI−TOF) ([M−2Cl]$^+$, m/z): Calcd for $C_{81}H_{71}N_{11}O_{11}RuZn$, 1611.37; Found for [M−2Cl]$^+$, 1612.1623.

Synthesis of 5,10,15-Tris(3',4',5'-trimethoxylphenyl)-20-[4'-hydroxylmethyl]phenyl]-21H,23H-porphyrin (*p*-CH$_2$OH Por)

3,4,5-Trimethoxylbenzaldehyde (5.00 g, 0.025 mol) and methyl 4-formylbenzoate

(1.39 g, 0.0085 mol) were added into 300 mL of propionic acid and the temperature of the mixture was raised to 120 °C. Then a solution of pyrrole (2.2 g, 0.0328 mol) in 50 mL of propionic acid was added dropwise into this mixture. When the addition was complete, the temperature was increased further to 140 °C and refluxing for 3 h. When the reaction was completed, the propionic acid was distilled off under reduced pressure. The remaining solid was purified by column chromatography ($CHCl_3$ as eluent). The purple product was dissolved in 250 mL THF. Under N_2, excess amount of lithium aluminium hydride was added into the solution, which was then stirring overnight. The resulting solution was filtered through celite. The filtrate was then washed with water and sodium bicarbonate solution several times until the green solution turned purple. The solvent was removed under reduced pressure and then purified by column chromatography. DCM/MeOH (v/v = 200 : 1). Yield 436 mg, 5.6%. ^{1}H NMR ($CDCl_3$) δ -2.782 (s, 2H), 3.96 (d, 18H, *J* = 4.4Hz), 4.17 (d, 9H, *J* =

2Hz), 5.03 (s, 2H), 7.47 (d, 6H, *J* = 1.2Hz), 7.23 (d, 2H, *J* = 8.4Hz), 8.19 (d, 2H, *J* = 8.0Hz), 8.85 (d, 2H, *J* = 4.8Hz), 8.95 (m, 6H).

Synthesis of 5,10,15-Tris(3',4',5'-trimethoxylphenyl)-20-[4'- benzylhydride]-21H,23H-porphyrin (*p*-CHO Por).

***p*-CH$_2$OH Por** (200 mg, 0.219 mmol) was oxidized by PCC (94 mg, 0.437 mmol) under N_2 at room temperature for 3 h. The solution was filtered through Celite, then the solution was washed with water and saturated sodium bicarbonate aqueous solution several times. The solvent was removed under reduced pressure and the

target compound was then purified by column chromatography with $CHCl_3$/MeOH (v/v = 30:1) as eluent. Yield 120 mg, 61%. ^{1}H NMR ($CDCl_3$) δ -2.802 (s, 2H), 3.96 (s,18H), 4.17 (s, 9H), 7.46 (s, 6H), 8.29 (d, 2H, *J* = 8.4 Hz), 8.44 (d, 2H, *J* = 8.4 Hz), 8.78 (d, 2H, *J* = 4.8 Hz), 8.95 (s, 6H).

Synthesis of Imidazole-Linked [(Porphyrin-Phen)Ru(bpy)$_2$][Cl]$_2$ (2)

***p*-CHO Por** (60 mg, 0.066 mmol), 1,10-phenanthroline-5,6-dione (60 mg, 0.286mmol) and excess amount of ammonium acetate was dissolved in 15 mL acetic acid. After refluxing overnight, the solvent was removed under reduced pressure. The residue was purified by column chromatography with $CHCl_3$/MeOH (v/v = 10 : 1) as eluent. The product obtained together with *cis*-Ru(bpy)$_2$Cl$_2$ (60 mg, 0.124 mmol) was dissolved in a mixture of THF (15 mL) and ethanol (15mL). The solution was then refluxed overnight. The solvent was removed and the residue was purified on neutral Al_2O_3 column with DCM/MeOH (v/v = 20:1) as eluent. Yield 45 mg, 66%. ^{1}H NMR (DMSO-d_6) δ −2.89 (s, 2H), 3.89 (d, 18H), 3.97 (d, 9H, *J* = 3.6 Hz), 7.39-7.41 (m, 2H), 7.50-7.53 (m, 6H), 7.58-7.60 (m, 2H), 7.60-7.61 (d, 2H, *J* = 6 Hz), 7.66-7.67 (m , 2H), 7.85- 7.90 (m, 4H), 8.10-8.14 (m, 2H), 8.14-8.19 (m, 2H), 8.21-8.33 (m 2H), 8.90- 8.92 (m, 6H), 8.92-9.07 (m, 9H), 9.15 (s, 2H). HRMS (MALDI-TOF) ([M−2Cl]$^+$, m/z): Calcd for $C_{86}H_{70}N_{12}O_9Ru$, 1516.62; Found for [M−2Cl]$^+$, 1516.9872.

Synthesis of Imidazole-Linked [(Zinc-Porphyrin-Phen)Ru(bpy)$_2$]-[Cl]$_2$(4)

Conjugates **3** (25 mg, 0.016 mmol) and excess amount of $Zn(OAc)_2.2H_2O$ were

dissolved in methanol and refluxed overnight. The residue was concentrated and purified by neutral Al_2O_3 with eluent DCM/MeOH (v/v=20:1). Yield 20 mg, 85%. ^{1}H NMR (DMSO-d_6) δ 3.92 (s, 18H), 4.01 (d, 9H, J = 3.2 Hz), 7.17-7.19 (d, 1H, J = 5.6Hz), 7.40-7.42 (m, 2H), 7.47-7.48 (m, 6H), 7.63 (s, 1H), 7.69 (s, 1H), 7.70-7.98 (m, 6H), 8.00- 8.16 (m 3H), 8.25-8.35 (m, 3H), 8.41-8.44 (m, 2H), 8.69-8.72 (m, 4H), 8.74- 8.77 (m, 2H), 8.79-8.94 (m, 8H), 9.23 (d, 2H, J = 5.2Hz). HRMS (MALDI−TOF) ([M−2Cl]$^+$, m/z): Calcd for $C_{86}H_{68}N_{12}O_9RuZn$, 1578.36; Found for [M−2Cl]$^+$, 1577.3113.

2.2 Photophysical Measurement.

UV-visible absorption spectra (200 - 1100 nm) were recorded by an HP Agilent UV-8453 spectrophotometer. Single-photon luminescence spectra were recorded using an Edinburgh Instrument FLS920 combined fluorescence lifetime and steady state spectrophotometer that was equipped with a visible to near-infrared- sensitive photomultiplier in nitrogen-cooled housing. The spectra were corrected for detector response and stray background light phosphorescence. The quantum yields of the compounds were measured by the comparative method and integrated sphere. [15] Singlet oxygen was detected directly by its phosphorescence emission at 1270 nm using an InGaAs detector on a PTI QM4 luminescence spectrometer. The emission quantum yields (Φ_{em}) of the test compounds were measured by comparative method and integrated sphere (H_2TPP = 0.11 and ZnTPP, Φ_{em} = 0.033 in toluene, Abs = 0.05). [25] Singlet oxygen quantum yield (Φ_Δ) were determined in chloroform by comparing

their singlet oxygen phosphorescence emission signals to that of a reference compound (H_2TPP, Φ_Δ = 0.55 in chloroform). [12]

2.3 Cell Culture.

Human cervical carcinoma HeLa cells were cultured in Dulbecco's Modified Eagle Medium (DMEM) supplemented with 10% fetal bovine serum (FBS) and 1% penicillin/streptomycin at 37 ℃ and 5% CO_2.

2.4 Flow Cytometric Cellular Uptake.

HeLa cells were seeded onto wells of a 6-well plate overnight. The cells were then incubated with 10 μM complexes **1-4** for 6 or 24 h at 37 ℃ and 5 % CO_2. Cells were then trypsinized and washed with 1X PBS for twice. The uptakes were then monitored with flow cytometer (BD FACSaria Cell Sorting System, BD Biosciences, China). The cells were excited by a 633 nm red laser, and the emissions were recordedusing a suitable optical filter (APC-Alexa Fluor ® 660 nm). At least 10000 events were analyzed for each measurement.

2.5 *In vitro* fluorescence imaging.

HeLa cells were seeded onto coverslip in 35-mm culture dishes overnight. The cells were then incubated with 10 μM complexes **1-4** for 20 h at 37 ℃ and 5% CO_2. For colocalization experiments, the cells were then washed with 1X PBS and stained with 50 nM Lysosome Tracker Green for 15 min. The emitted fluorescent signals of

complexes and the tracker were examined with an inverted fluorescence microscope (Zeiss Axio Observer Z1, Zeiss, Germany) equipped with a UV lamp, mercury bulbs and a customized fluorescence filter (excitation wavelength = 365 nm, emission wavelength = 610 nm). A 63X oil immersion objective was used for imaging.

2.6 Photo-cytotoxicity assay.

The PDT cytotoxicity assay was performed according to standard methods. In general, HeLa cells (3×10^3/ well) were incubated in 96-well plates 24 hours prior to exposure to drugs. The cells were treated with samples **1-4** in the dark overnight. Afterwards, the cells were exposure to yellow light (1-4 J / cm^2) produced from a 400 W tungsten lamp fitted with a heat-isolation filter and a 550 nm long-pass filter. The fluence rate was 6 mW/cm^2. Cell viability was determined by the MTT reduction assay at 24 h post-PDT. [27] The cell monolayers were rinsed twice with PBS and then incubated with 50 μL MTT solution (0.5 mg / mL) at 37°C for 3h. Then the media were removed, and 100 μL of DMSO solubilizing reagent was added and shaked for 30 minutes to dissolve the formed formazan crystals in living cells. The absorbance was measured at dual wavelength, 540 nm and 690 nm, on a Labsystem Multiskan microplate reader (Merck Eurolab, Switzerland). Each dosed concentration at individual light exposure was performed in quadruplicate wells for the PDT assay.

3 Results and Discussion

3.1 Linear-Induced Photophysical Properties.

The UV-visible absorption spectra of the four conjugates (**1** to **4**) were measured in various solvents ranging from the non-polar chloroform ($CHCl_3$) to the polar acetonitrile (MeCN), ethanol (EtOH) and deionised (DI) water (Figure S13). The absorption band at 288 nm was observed in all four conjugates and is assigned to the π-π* transition of the bipyridine (bpy) ligand of Ru(II) complex. The strong porphyrin Soret band is located at ~420 nm for the free-base porphyrin conjugates (**1**, **2**) and ~425 nm for the Zn(II) porphyrin conjugates (**3, 4**). The absorption bands observed in 500-700 nm correspond to the porphyrin Q bands, with four bands seen in conjugates **1** and **2**, and two bands in conjugates **3** and **4**, due to the Zn(II) coordination of the porphyrins. It should be pointed out that the Ru(II)-polypyridyl moiety should absorb at around 450 nm (^{1}MLCT band). However, because its molar absorptivity is only one-tenth of that of the Soret band, it would appear at most as a weak shoulder associated with the porphyrin Soret band. It became enhanced significantly in nonpolar solvents, thus confirming the MLCT character of this shoulder absorption.

[16] The Soret band of the Zn(II) porphyrin-Ru conjugates **3**-**4**, shows substantially diminished intensity when compared to the corresponding free-base porphyrins. The Zn(II) metalation of the porphyrin significantly raises its π* energy level, making it the highest-excited state in these conjugates.

In conjugates **1** and **2**, the porphyrin Soret band exhibits a slight hypsochromic shift with increasing solvent polarity, thus demonstrating solvatochromism. In the Zn(II) porphyrin conjugates **3** and **4**, this solvatochromic trend became less obvious. Multiple factors can influence solvatochromism, such as the polarizability difference

between the ground and excited states, dipole moment changes on excitation, and hydrogen bonding in protic solvents. [17]

The emission spectra of the four porphyrin-Ru(II) conjugates, excited at ~420 nm, were also measured in the following solvents of increasing polarity: $CHCl_3$, MeCN, EtOH and DI water (Fig. S14). The free-base porphyrin-Ru(II) conjugates, **1- 2**, showed two intense emission bands at ~655 nm and ~718 nm, which are assignedto the porphyrin Q (0-0) and Q (0-1) transitions, respectively. The complexation of the porphyrin by Zn(II) raised the π^* excited state energy of the porphyrin, resulting in the observed blue-shift of the emission bands by ~50 nm relative to the free-base porphyrin conjugates (**1** and **2**) to ~610 nm and ~660 nm, respectively. The intensity ratio between these two emission peaks (labelled a and b in Fig. 2) changed as well, indicating that the structure of the porphyrin is no longer square planer but somewhat twisted. The emission quantum yields of these conjugates, measured relative to the reference standard of 5,10,15,20-tetraphenylporphyrin (H_2TPP, Φ_{em} = 0.11 in toluene) and the corresponding Zn(II) porphyrin (ZnTPP, Φ_{em} = 0.033 in toluene), [18] are given in Table 1.

The first observation from Fig. 2 is that the emission intensities of the free-base porphyrin conjugates (**1** and **2**) are significantly higher than those of the Zn(II) porphyrin conjugates (**3** and **4**), which suggests that the free-base porphyrins are getting energy from the Ru(II) complex. The energy transfer from porphryin to Ru(II)was enhanced in more polar solvents. This is attributed to the dipole moment change between the ground and the excited states. [19] As a reduction in dipole moment in

the excited state is expected, the excited state should become less stabilized than the ground state in polar solvents. [20-22]

To further evaluate the energy transfer between porphyrin and the Ru(II) complex, the emission spectra of the four conjugates in ethanol were measured under different excitation wavelengths at room temperature (Fig. 2) to probe the triplet states of the porphyrin/Ru moieties. When excited from 400 to 460 nm, the free-base porphyrin conjugates (**1** and **2**) showed only emission from the porphyrin. However, when the excitation was changed to 460 nm, only Zn-Por-Ru give emission band that correspond to the ^{1}MLCT band of the Ru(II). The shoulder emission at *ca.* 600 nm became enhanced. This shoulder emission is assigned to the Ru(II) ^{3}MLCT excited state. The finding is similar to the results of Kon et. al., i.e. energy is transferred from the lowest singlet excited state of Zn. [23,24]

As shown by Kon et al., the excited state energy levels of porphyrin and ruthenium units are comparable and can be easily reversed by the introduction of metal ion coordination to the porphyrin ring. In our four porphyrin-based conjugates with two linkers, one flexible and one more rigid, similar observations were found: the emission quantum yields, Φ_{em}, of the free-base porphyrin-ruthenium conjugates **1** and **2** are 3.31% and 2.64%, respectively, in chloroform (Table 1). With Zn(II) coordination at the porphyrin, the emission quantum yields of these conjugates (**3**: Φ_{em} = 1.91%, and **4**: Φ_{em} = 1.50%, in chloroform, Table 1), as well as their $^{1}O_2$ quantum yields, were seen to drop considerably, showing a reversal of energy transfer. (Figure S15 and Table 1) Changing the linker between the porphyrin and Ru moieties does

not change the emission quantum yield. In the solvatochromism studies of the emission of conjugates **1**-**4**, the emission intensity enhancement observed in free-base porphyrin-Ru(II) conjugates, **1**-**2** is related to the decreasing solvent polarity (MeCN ~ EtOH > $CHCl_3$). However, in zinc-porphyrin-Ru(II) conjugates, **3**-**4**, the observed emission solvatochromism is different, especially in complex **3** with flexible linker, the emission of **3** in polar solvent is greater than non-polar solvent. From the emission spectra shown in Fig 2 and Fig. S14, the excitation wavelength dependency suggests that porphyrin emission is involved. The emission spectra of the four conjugates **1**-**4** excited at 288 nm, which is assigned to the π π^* transition of the bipyridine moiety, were also measured. As expected, conjugates **1** and **2** showed much stronger porphyrin emission, when compared with conjugates **3** and **4** (Fig. S16). Meanwhile, excitation spectra of these conjugates (**1**-**4**) monitored at 661 nm, which correspond toporphyrin emission, was measured as well. Only conjugates **1** and **2** shown peak at 288 nm, which further indicates the energy transfer is from Ru moiety to porphyrin moiety. To further study the photochemistry of conjugates **1**-**4**, the emission lifetimes of **1**-**4** were measured and shown in Table S1. In Table S1, Zn(II) porphyrin-Ru(II) conjugates **3** and **4** exhibit shorter emission lifetimes and lower quantum yields, as compared to their free-base counterparts, **1** and **2**. The emission lifetimes measured from the four conjugates (in chloroform, acetonitrile and ethanol) in the range of ~11- 30 ns are attributed to emission from the porphyrin moiety (τ ~ 10 - 50 ns, typically), which became shortened upon Zn(II) coordination in conjugates **3** and **4**. Interestingly, lifetime measurement of conjugates **3** and **4** in water showed one longer

emission decay curve with a lifetime of *ca*. 0.1 ms. This long emission is attributed to the ruthenium moiety, which usually exhibits a relatively long lifetime (ns - μs). [27] Since ruthenium moiety has better solubility in water and it is getting energy from the porphyrin in these conjugates, thus results in longer observable lifetime in water.

3.2 Confocal Imaging of Conjugates **1-4**.

The subcellular localization of the conjugates has been examined in HeLa cells after incubation for 24 hours. The four conjugates are seen to localize in the lysosome (Fig. 3). To confirm their subcellular localization, co-staining experiments using commercially available organelle-specific markers were performed. After 6 hours of incubation with these conjugates, the lysosome-specific marker (Invitrogen, Lysotracker green, 1 mg / mL) was then added. In Fig. 3, the images in the right panel, which represent the merged images (yellow) of the four porphyrin-Ru(II) conjugates (left panel, red) with those from the Lysotracker green (middle panel, green), clearly show the co-localization of the Lysotracker green with these conjugates in the lysosome. The lysosome localization of these conjugates is presumably due to their acidic nature as shown by their pKa values at 3.4 - 3.8.

3.3 Dark and photocytotoxicity of conjugates **1-4**.

The IC_{50} values of **1-4** in dark have been evaluated in HeLa cells. The variation of the linker induced different dark cytotoxicity properties. **2** and **4** with the rigid linker were found to be less toxic in dark compared to **1** and **3** (IC_{50} of **1** = 50 μM, **2** =

125 μM, **3** = 48 μM and **4** = 135 μM), since the cellular uptake of **1** and **3** is greater than **2** and **4** (Table 2, Fig. S17, S18). The complexation of Zn does not seem to be affected the dark toxicity (IC_{50} of **1** and **3**, **2** and **4** are similar).

According to the dark toxicity results, we evaluated the light toxicity of **1**–**4** with the maximum dosed concentration at 10 μM. With light excitation, the free-porphyrin Ru(II) conjugates **1** and **2** showed much more toxic than zinc-porphyrin Ru(II) conjugated **3** and **4** respectively. This trend is quite consistent with the measured singlet oxygen quantum yields of these conjugates (Table 1), where the excitation energy derived from the Ru(II) chromophore in conjugates **1** and **2** was channelled to the generation of $^1O_2$, presumably resulting in the higher photocytotoxicity observed. (Figure 4)

4. Conclusions

In conclusion, we have synthesized four new porphyrin-Ru(II) conjugates and their absorption and emission spectra were measured. From these photophysical data, the energy migration between the porphyrin and the Ru(II) chromophores is affected by the Zn(II) coordination of the porphyrin moiety, with no obvious effect from the two types of linkers investigated. The significantly higher $^1O_2$ quantum yield was observed for the free-base porphyrin conjugates (**1** and **2**) compared to their Zn(II) counterparts, and is interpreted to be the result of the additional energy transfer from the excited Ru(II) chromophore to the porphyrin triplet state, which sensitize the $^1O_2$ generation. However, the cell uptake rate of these conjugates with similar molecular

weight and charge is influenced by the linker.

No differential subcellular localization was seen among these four conjugates. They were all localized in the lysosome due to the acidic pKa. The photocytotoxicity observed in these conjugates is apparently more influenced by their $^1O_2$ quantum yield. The phototoxicity effect of free porphyrin Ru(II) conjugates **1** and **2** is much stronger than zinc-porphyrin Ru(II) conjugated **3** and **4**. However, **2** is much less toxicthan **1** in dark, (the uptake rate of **1** and **2** is similar), we can conclude that metal-free porphyrins with a rigid linker for Ru(II) conjugate **2** is the best PDT agents out of other three Ru complexes in this study. Nonetheless, this study reaffirms the effects oflinker on cells, which is an important design parameter for the new generation of PDTagents based on porphyrin-metal complex conjugates.

Acknowledgements

This work was funded by grants from The Hong Kong Research Grants Council (HKBU 203112), EPSRC and Hong Kong Baptist University. HKBU and HK PolyU Joint Research Programme (RC-ICRS/15-16/02F-WKL02F-WKL and RC-ICRS/15-16/02D- KWJ).

5 References

[1] J. F. Lovell, T. W. B. Liu, J. Chen and G. Zheng, Chem. Rev. 110 (2010), 2839-2857.

[2] T. J. Dougherty, C. J. Gomer, B. W. Henderson, G. Jori, D. Kessel, M. Korbelik, J. Moan and Q. Peng, J. Natl. Cancer Inst. 90 (1998) 889-905.

[3] R. K. Pandey, G. K. Zheng, Porphyrins as photosensitizers in photodynamic therapy, In: K. M. Kadish, K. M. Smith, R. Guilard (Eds.), The Porphyrin Handbook, Academic Press, Boston, 2000, pp. 157-230.

[4] S. M. Z. Hossain, S. M. G. Azam and S. M. E. Babar, Mol. Cell. Toxicol. 2 (2006) 1-6.

[5] K. Ogawa and Y. Kobuke, Anti-Cancer Agents Med. Chem. 8 (2008) 269-279.

[6] C. T. Poon, P. S. Chan, C. Man, F. L. Jiang, R. N. S. Wong, N.-K. Mak, D. W. J. Kwong, S. W. Tsao and W. K. Wong, J. Inorg. Chem. 104 (2010) 62-70.

[7] A. E. Friedman, J. C. Chambron, J. P. Sauvage, N.J. Turro and J. K. Barton, J. Am. Chem. Soc. 112 (1990) 4960-4962.

[8] R. M. Hartshorn and J. K. Barton, J. Am. Chem. Soc. 114 (1992) 5919-5925.

[9] K. L. Haas and K. J. Franz, Chem. Rev. 109 (2009) 4921-4960.

[10] C. Mari, V. Pierroz, S. Ferrari and E. Gasser, Chem. Sci. 6 (2015) 2660-2686.

[11] B. S. Howerton, D. K. Heidary and E. C. Glazer, J. Am. Chem. Soc. 134 (2012) 8324-8327.

[12] J. X. Zhang, J. W. Zhou, C. F. Chan, T. C. Lau, D. W. Kwong, H. L. Tam, N. K. Mak, K. L. Wong and W. K. Wong, Bioconjug. Chem. 23 (2012) 1623-1638.

[13] A. Aguirre-Soto, C. H. Lim, A. T. Hwang, C. B. Musgrave and J. W. Stansbury, J.

Am. Chem. Soc. 136 (2014) 7418-7427.

[14] S. Rau, D. Walther and J. G. Vos, Dalton Trans. 9 (2007) 915-919.

[15] A. Hagfeldt and M. Gra ̈tzel, Acc. Chem. Res. 33 (2000) 269-277.

[16] N. D. McClenaghan, Y. Leydet, B. Maubert, M. T. Indelli and S. Campagna, Coord. Chem. Rev. 249 (2005) 1336-1350.

[17] I. Renge and K. Mauring, Spectrochim. Acta Pt. A: Mol. Biomol. Spec. 102 (2013) 301-313.

[18] I. Gupta and M. Ravikanth, J. Chem. Sci. 117 (2005) 161-166.

[19] S. Fantacci, F. D. Angelis and A. Selloni, J. Am. Chem. Soc. 125 (2003) 4381-4387.

[20] M. T. Indelli, C. A. Bignozzi and F. Scandola, Inorg. Chem. 37 (1998) 6084-6089.

[21] C. E. B. Evans, M. L. Naklicki, A. R. Rezvani, C. A. White, V. V. Kondratiev and R. J. Crutchley, J. Am. Chem. Soc., 120 (1998) 13096-13103.

[22] W. Kaim and S. Kohlmann, Inorg. Chem. 25 (1986) 3306-3310.

[23] H. Kon, K. Tsuge, T. Imamura, Y. Sasaki, S. Ishizaka, N. Kitamura and M. Kato, Dalton Trans. 12 (2008) 1541-1543.

[24] H. Kon, K. Tsuge, T. Imamura, Y. Sasaki, S. Ishizaka and N. Kitamura, Inorg. Chem. 45 (2006) 6875-6883.

[25] M. D. Ward, Coord. Chem. Rev. 250 (2006) 3128-3141.

[26] S. Ji, W. Wu, W. Wu, P. Song, K. Han, Z. Wang, S. Liu, H. Guo, J. Zhao, J. Mater. Chem., 20 (2010) 1953-1963.

[27] N. K. Mak, K. M. Li, W. N. Leung, N. S. Wong, D. P Huang, M. L. Lung,

Y. K. Lau, C. K. Chang, Biochem Pharmacol., 68 (2004) 2387-2391.

Fig captions

Figure 1. The molecular structures of free (**1,2**) or zinc (**3,4**) based porphyrin-ruthenium (II) complexes.

Figure 2 Emission spectra of conjugates (a) **1** (left) and **2** (right), and (b) **3** (left) and **4** (right), obtained at various excitation wavelengths in EtOH (10^{-6} M). The spectra were all measured at room temperature. (λ_{ex} = 400-460 nm)

Figure 3 Confocal fluorescent microscopic images of the free-base porphyrin-Ru(II) conjugates **1** (a), **2** (b), and Zn(II) porphyrin-Ru(II) **3** (c), **4** (d) (dosed concentration = 10 μM, λ_{ex} = 365 nm, incubation time = 24 h), together with their lysosome tracker green and their corresponding bright field overlay images

Figure 4 Photocytotoxicity of free-base porphyrin-Ru(II) conjugates **1** (a), **2** (b), and Zn(II) porphyrin-Ru(II) conjugates **3** (c), **4** (d), were obtained using 1-10 μM of conjugates and various light doses from 1 to 4 J/cm^2 after incubation for 24 h in HeLa cells.

Table 1. Photophysical Properties of the Porphyrin-Ru(II) Conjugates, **1-4**.

Compd	λ_{abs}/nm (logε)				Φ_{em}/%[a]				Φ_{Δ}/%[b]	pKa[c]
	$CHCl_3$	MeCN	EtOH	DI water	$CHCl_3$	MeCN	EtOH	DI water		
1	288(5.08) 424(5.61)	286(4.83), 419(5.46)	286(4.87), 419(5.46)	286(4.18), 419(4.17)	3.31	3.73	5.19	3.25	42.8	3.79
2	288(4.93) 425(5.41)	287(5.03), 420(5.21)	287(4.97), 420(5.17)	286(4.97), 432(4.46)	2.64	3.22	7.50	3.61	50.1	3.37
3	289(4.21) 426(4.73)	286(4.93), 425(5.10)	287(4.90), 425(5.01)	286(4.61), 432(4.16)	1.91	1.37	2.01	2.34	29.2	3.73
4	289(4.59) 427(5.29)	287(4.76), 426(4.91)	287(5.11), 427(5.34)	286(4.90), 435(4.66)	1.50	1.21	2.56	2.93	17.5	3.36

[a] Emission quantum yields of conjugates **1-4** (λ_{em} = 550−800 nm, λ_{ex} = 420 nm).
[b] $^1O_2$ quantum yields of conjugates **1-4** (λ_{ex} = 420 nm).
[c] pK_a value of conjugates **1-4** obtained from the variation of the ratio of emission intensity at maximum *vs*. pH (295 K, HEPES buffer, 1% DMSO, λ_{ex} = 420 nm).

Table 2. The IC_{50} of dark and light cytotoxicity of 1-4

Compd.	IC_{50} μM		
	Dark[a]	Light Dose[b]	
		1 J	2 J	4 J
1	50	9.6	7.6	5.1
2	125	9.7	9.5	4.9
3	48	45	30	20
4	135	20	15	14

[a] Dark cytotoxicities (IC_{50}) of compounds **1-4** toward HeLa cells were determined from the dose−response curve obtained after 24 h incubation with various concentrations of the conjugates.

[b] Photocytotoxicities of compounds **1-4** toward HeLa cells was determined under various light doses.

.

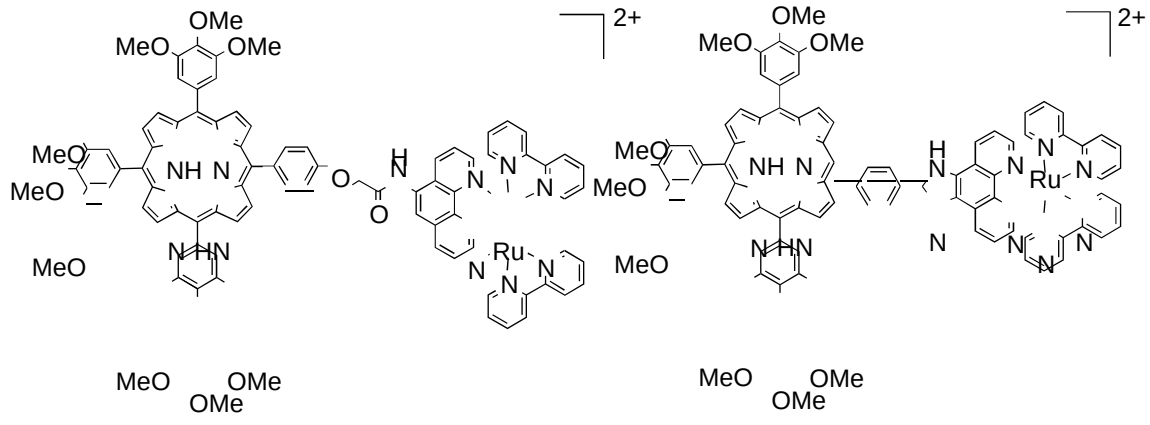

1 **2**

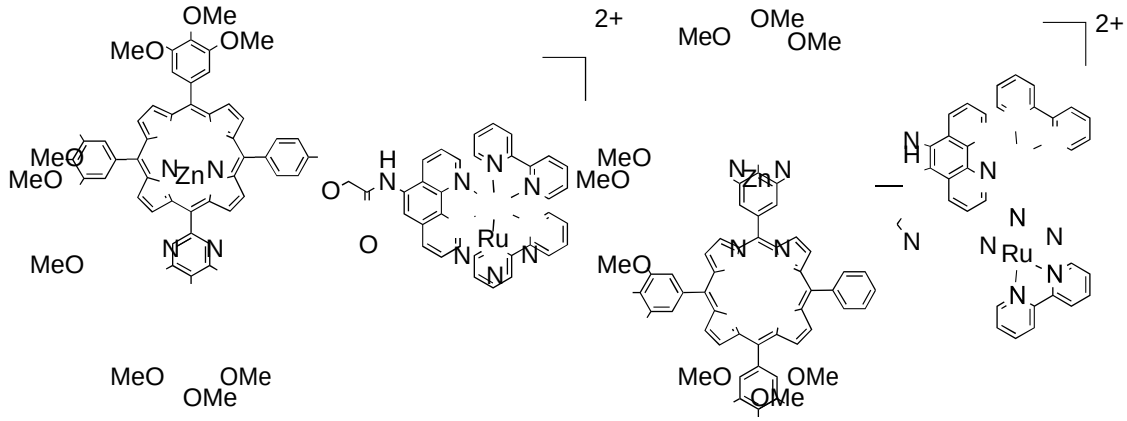
OMe
MeO
OMe
MeO
MeO
N
Zn
N
N
N
MeO
MeO
OMe
OMe
2+
H
N
O
O
N
N
N
Ru
N
N
MeO
MeO
MeO
OMe
OMe
N
Zn
N
N
N
MeO
MeO
OMe
OMe
2+
N
H
N
N
N
Ru
N
N
N

3 **4**

Figure 1

a)

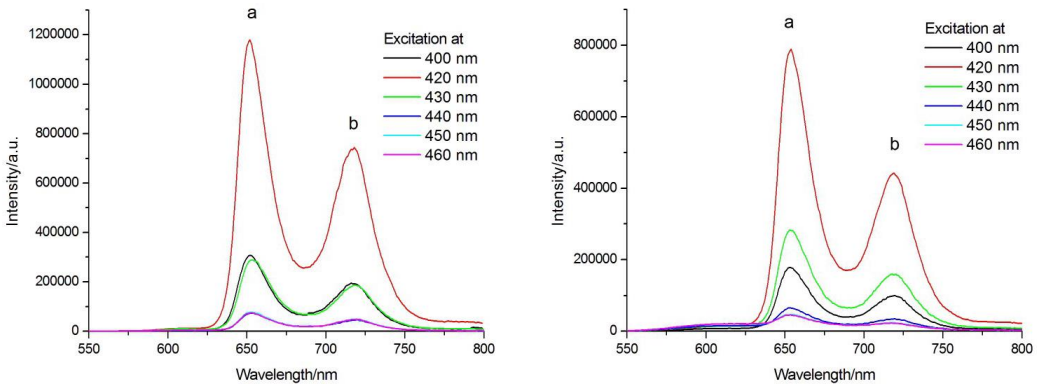
a
b
Excitation at
400 nm
420 nm
430 nm
440 nm
450 nm
460 nm
Intensity/a.u.
Wavelength/nm

b)

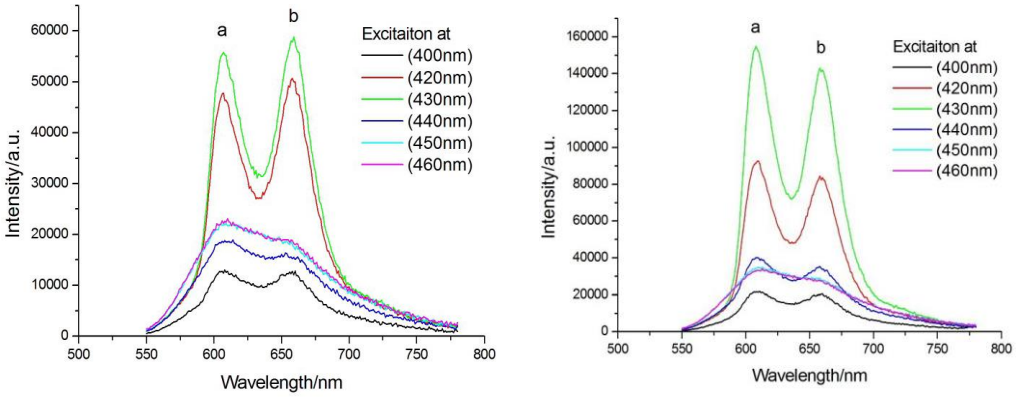
a
b
Excitaiton at
(400nm)
(420nm)
(430nm)
(440nm)
(450nm)
(460nm)
Intensity/a.u.
Wavelength/nm

Figure 2

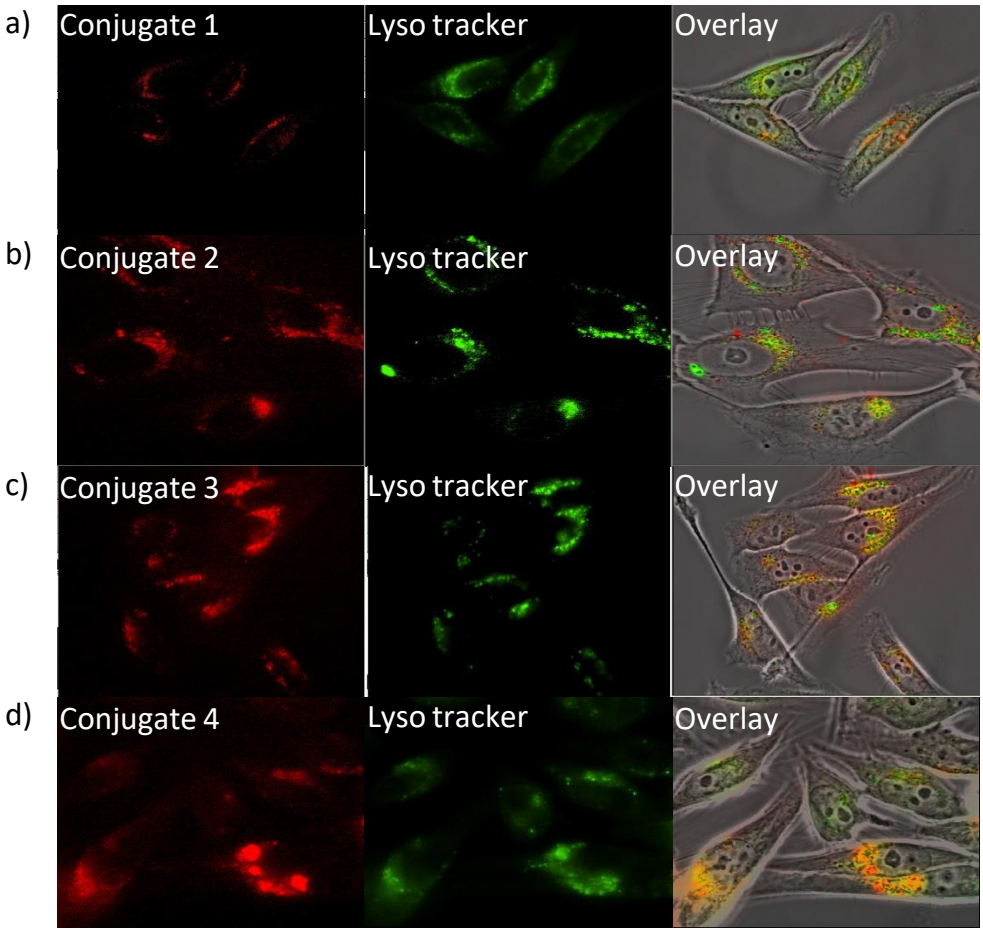
a)
Conjugate 1
Lyso tracker
Overlay
b)
Conjugate 2
Lyso tracker
Overlay
c)
Conjugate 3
Lyso tracker
Overlay
d)
Conjugate 4
Lyso tracker
Overlay

Figure 3

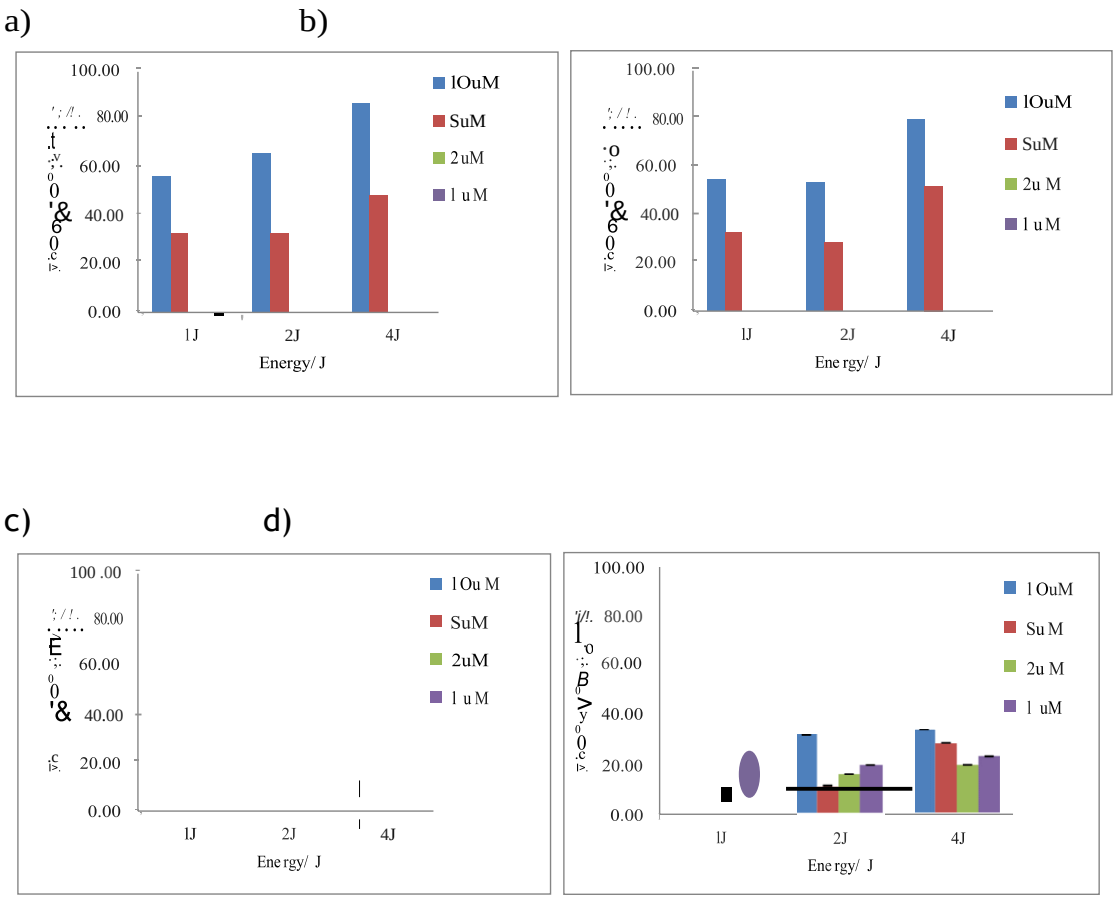
a)
b)
100.00
80.00
60.00
40.00
20.00
0.00
lOuM
SuM
2uM
1 uM
1J
2J
4J
Energy/ J
100.00
80.00
60.00
40.00
20.00
0.00
lOuM
SuM
2u M
1 uM
1J
2J
4J
Ene rgy/ J
c)
d)
100 .00
80.00
60.00
40.00
20.00
0.00
1 Ou M
SuM
2uM
1 uM
1J
2J
4J
Ene rgy/ J
100.00
80.00
60.00
40.00
20.00
0.00
1 OuM
Su M
2u M
1 uM
1J
2J
4J
Ene rgy/ J

Figure 4

Supporting Information

for

Excitation energy transfer in Ruthenium (II)-porphyrin conjugates led to enhanced emission quantum yield and $^1O_2$ generation

Jie Pan,[a] Lijun Jiang,[a] Chi-Fai Chan,[a] Tik-Hung Tsoi,[b] Kwok Keung, Shiu,*[a] Daniel W. J. Kwong,*[a] Wing-Tak Wong,*[b] Wai-Kwok Wong,*[a] and Ka-Leung Wong*[a]

[a] Department of Chemistry, Hong Kong Baptist University, Kowloon Tong, Hong Kong SAR;
Tel: 852 34117509, Email: wkwong@hkbu.edu.hk.
Tel: 852 34112370, Email: klwong@hkbu.edu.hk.
Tel: 852 34117387, Email: dkwong@hkbu.edu.hk.
Tel: 852 34117346, Email: kkshiu@hkbu.edu.hk.
[b] Department of Applied Biology and Chemical Technology, Hong Kong Polytechnic University, Hung Hom, Hong Kong SAR.
Email:bcwtwong@polyu.edu.hk

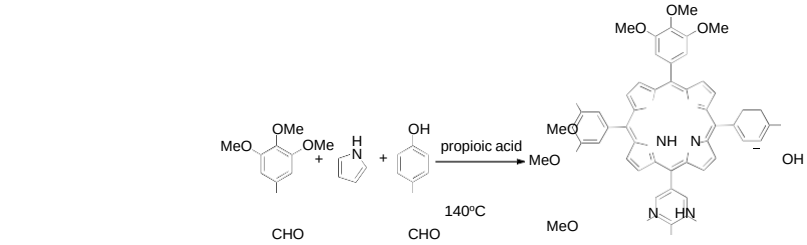

Por-OH

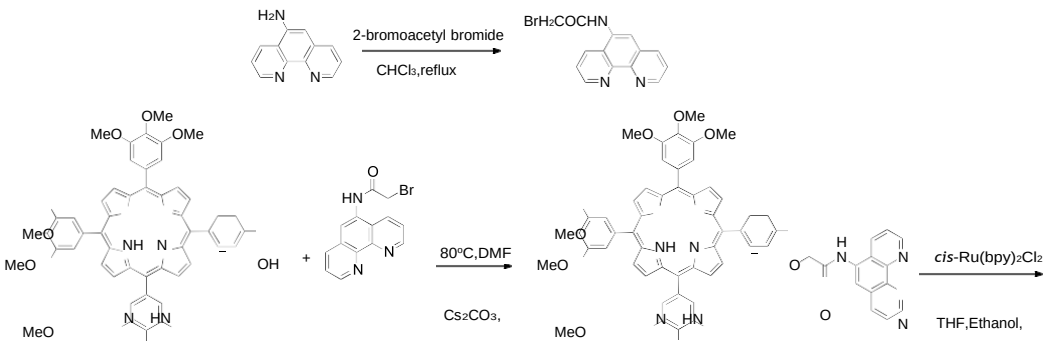

Por-OH **L1**

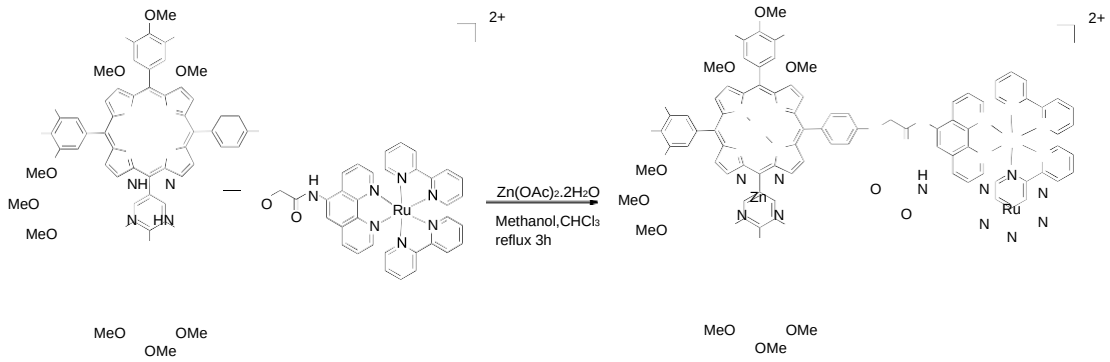

1 **3** **3** **1**

3

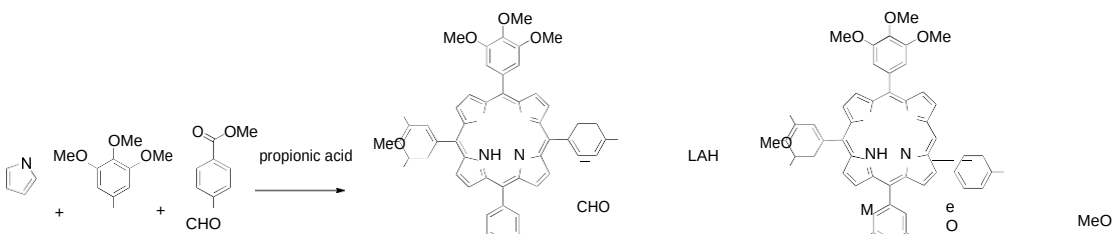

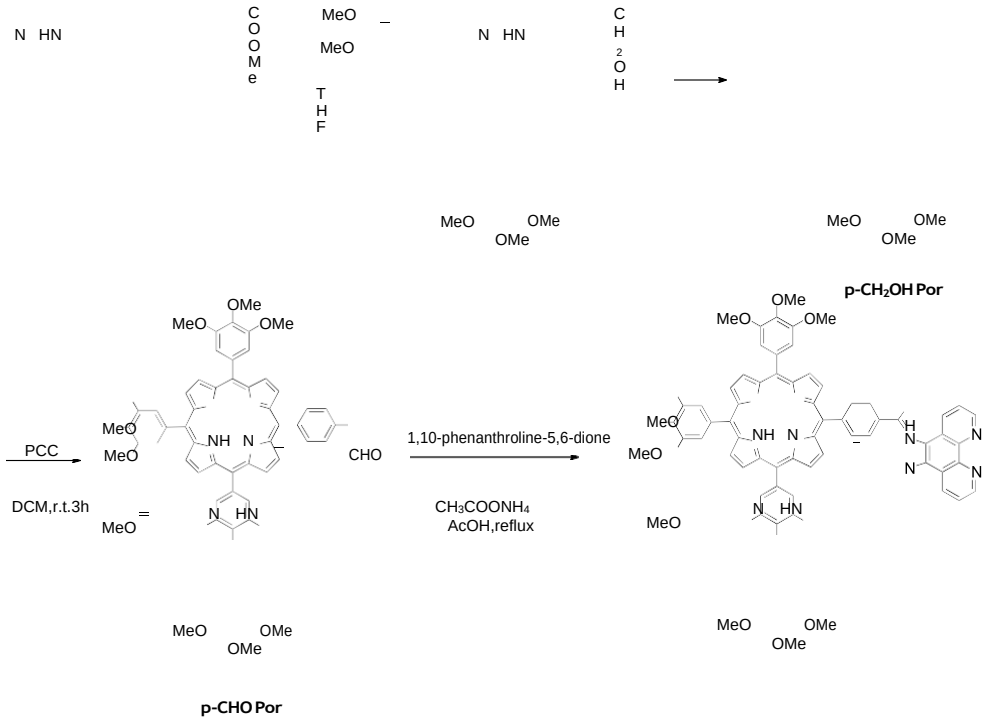
N HN
COOMe
MeO
MeO
THF
N HN
CH2OH
MeO OMe
OMe
MeO OMe
OMe
p-CH2OH Por
PCC
DCM,r.t.3h
CHO
1,10-phenanthroline-5,6-dione
CH3COONH4
AcOH,reflux
MeO OMe
OMe
p-CHO Por

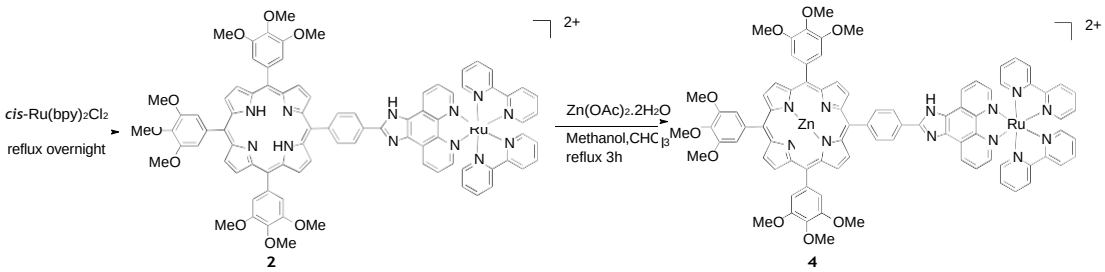

Scheme S1. The synthetic routes for conjugates **1-4**

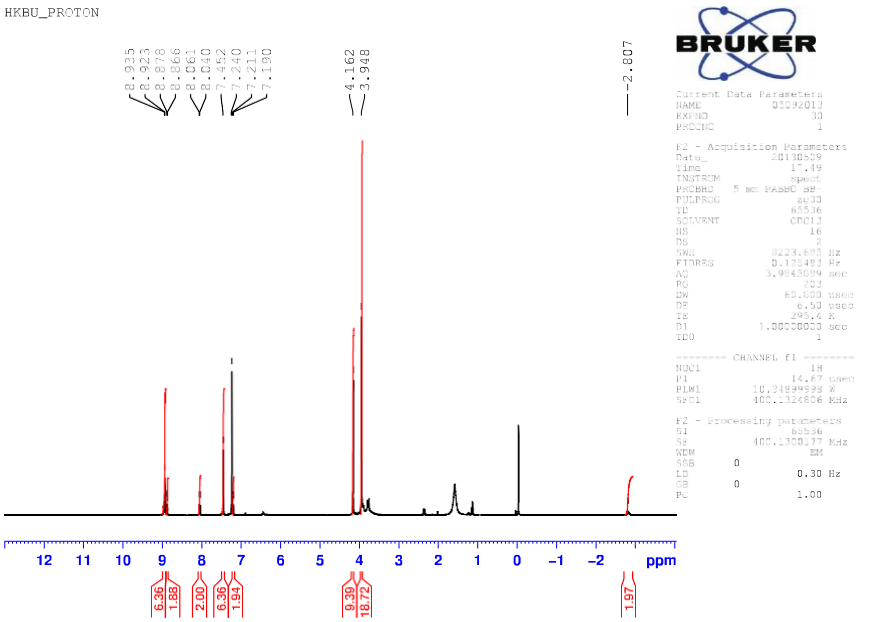

Figure S1. ^{1}H NMR Spectrum of **Por-OH**

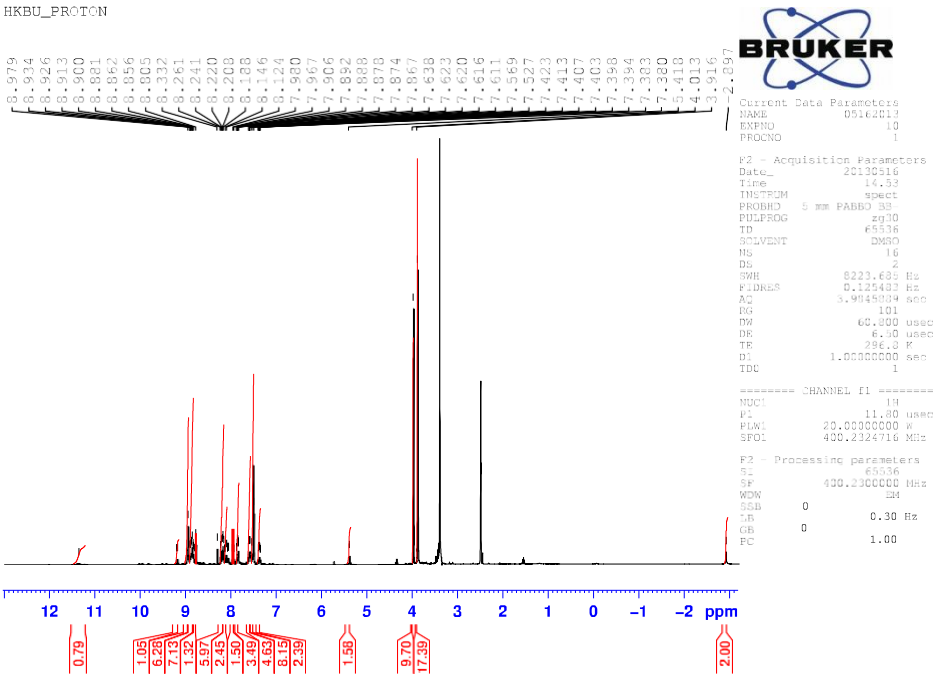

Figure S2. ^{1}H NMR Spectrum of $\mathbf{L_1}$

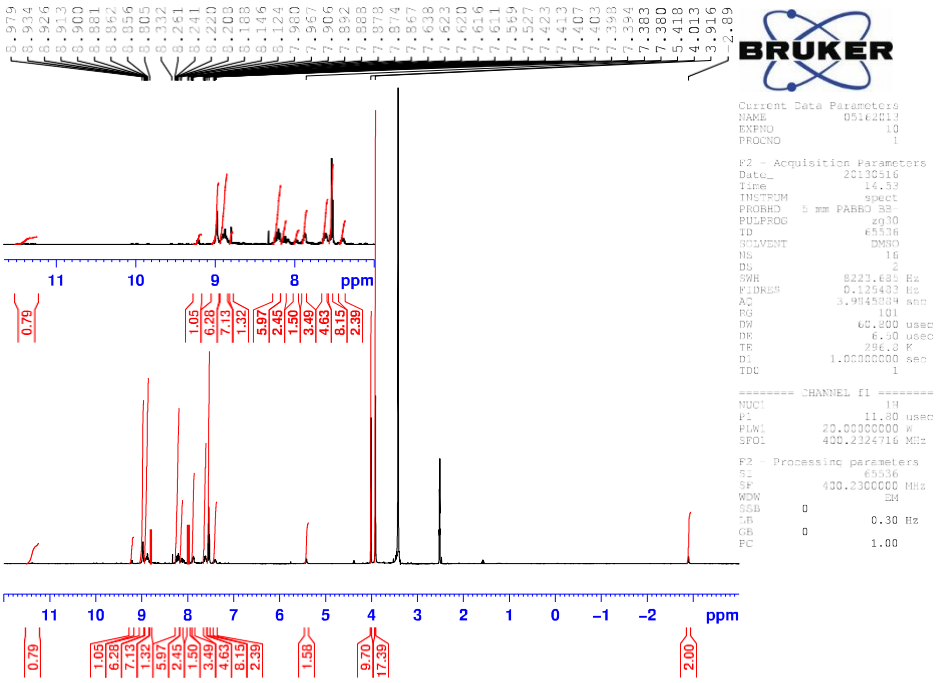

Figure S3. ^{1}H NMR Spectrum of conjugate **1.**

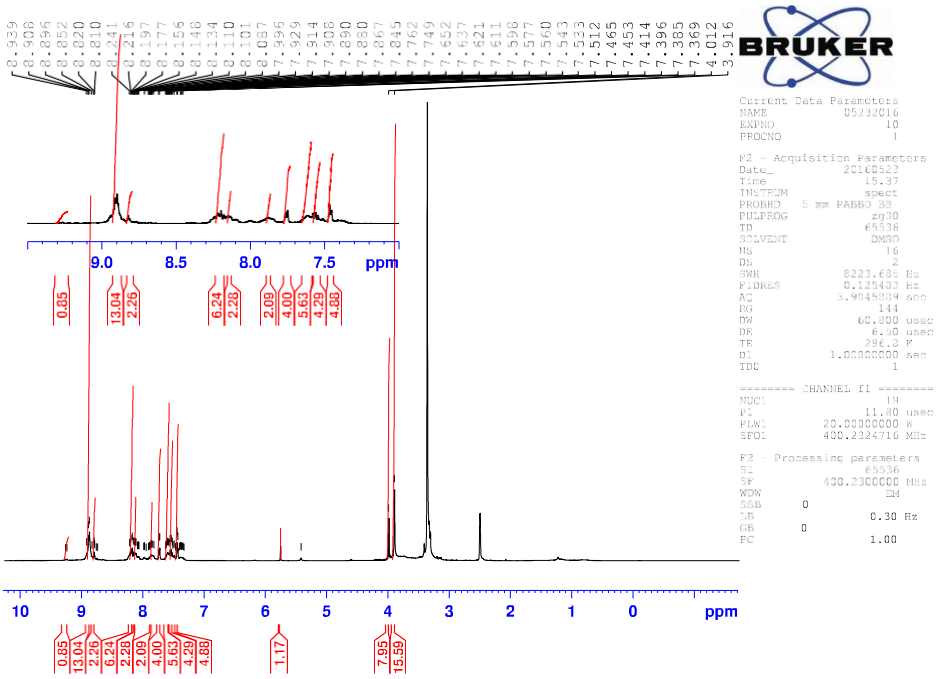

Figure S4. ^{1}H NMR Spectrum of conjugate **3.**

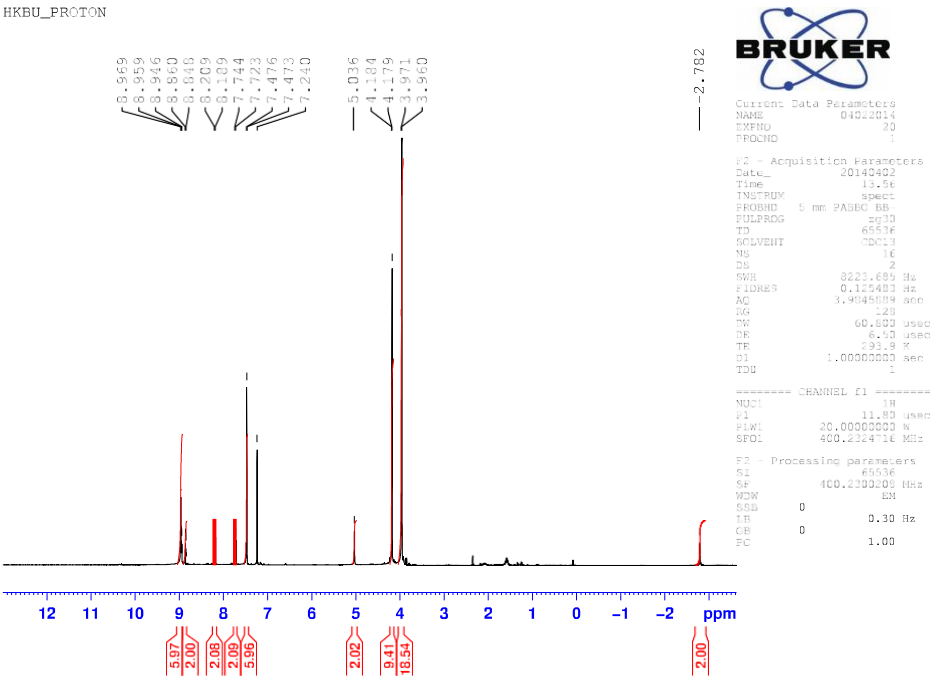

Figure S5. ^{1}H NMR Spectrum of ***p*-CH_2OH Por.**

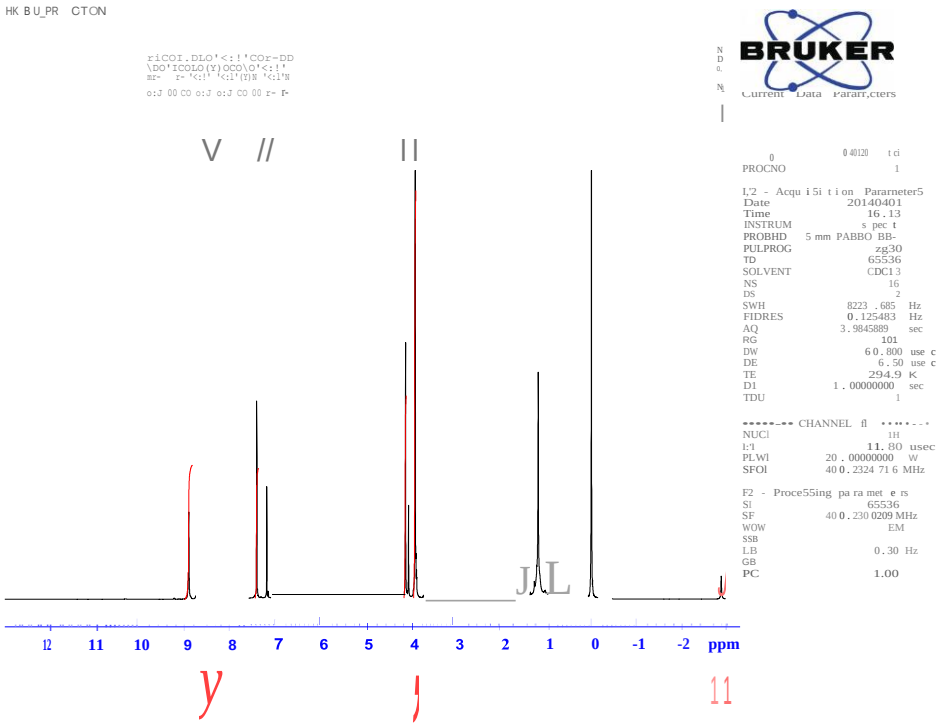

Figure S6. ^{1}H NMR Spectrum of ***p*-CHO Por.**

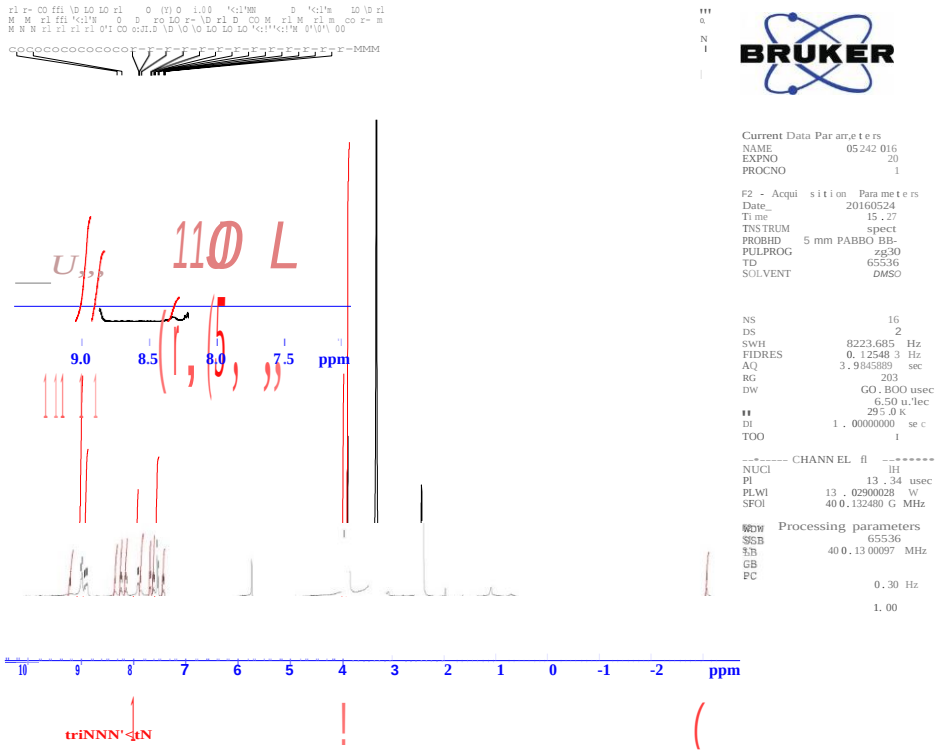

Figure S7. ^{1}H NMR Spectrum of conjugate **2.**

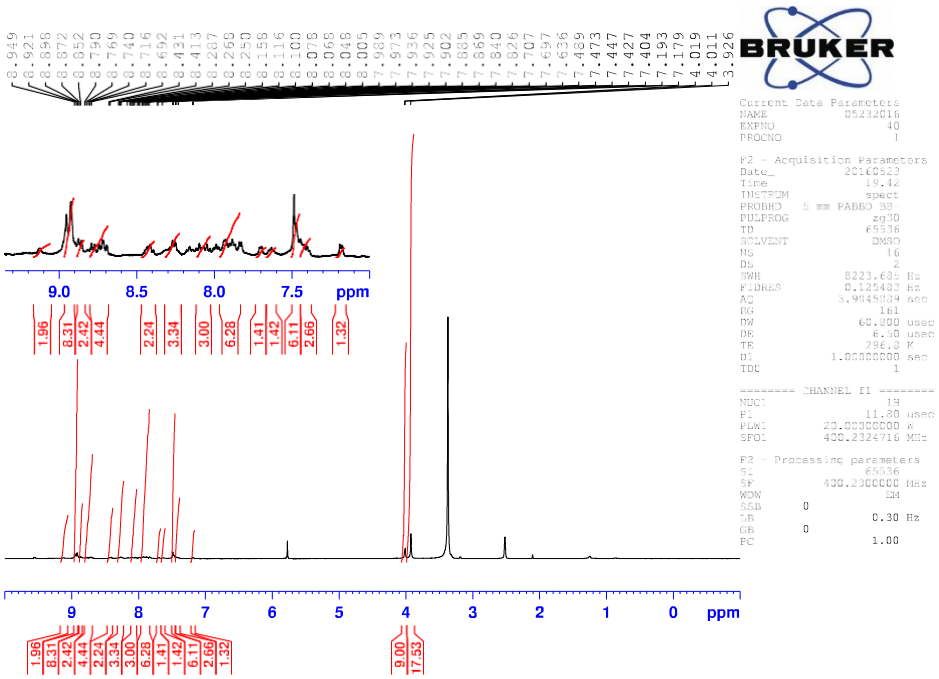

Figure S8. ^{1}H NMR Spectrum of conjugate **4.**

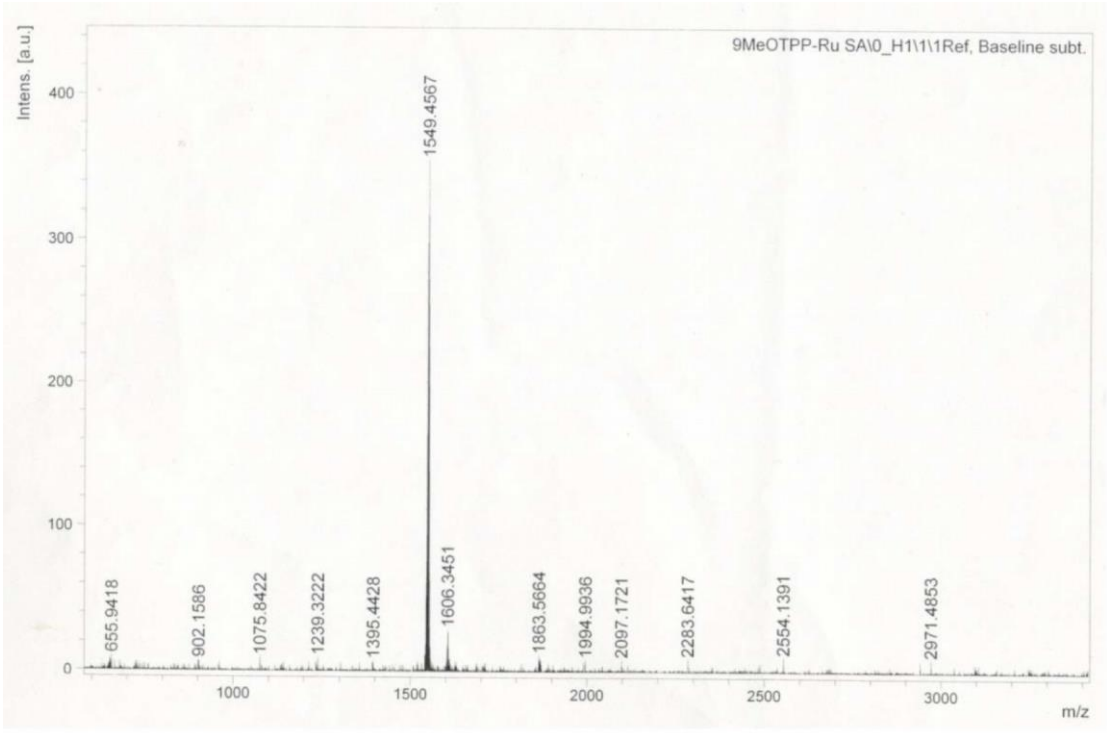

Figure S9. HR-MALDI-TOF Spectrum of conjugate **1.**

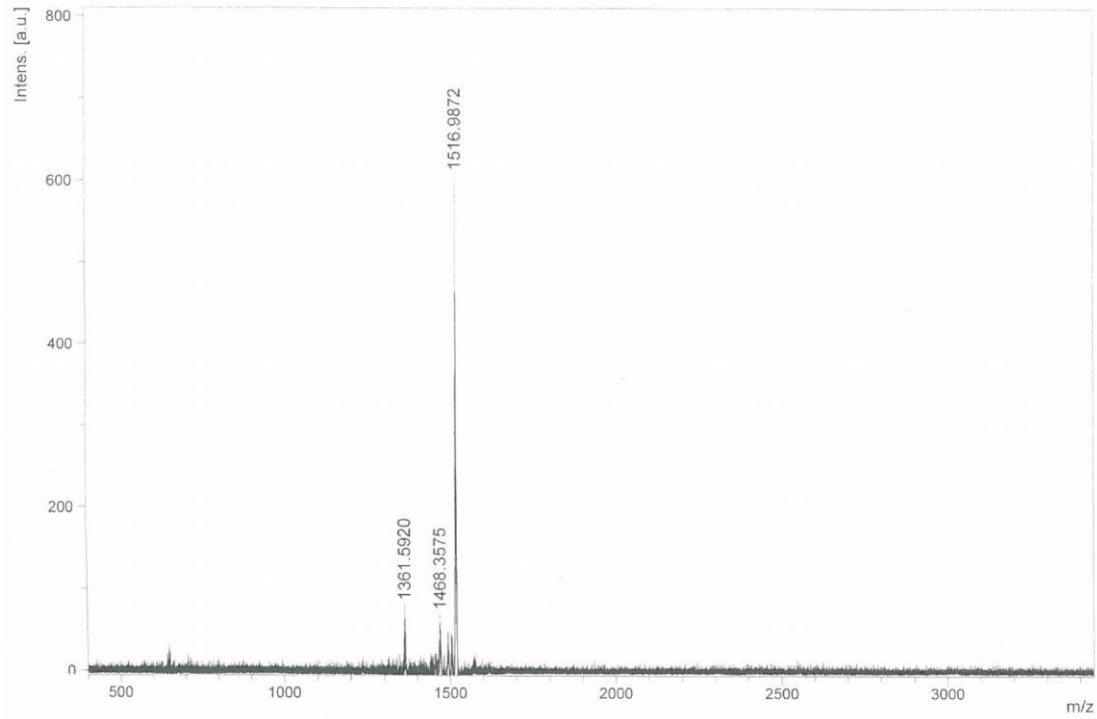

Figure S10. HR-MALDI-TOF Spectrum of conjugate **2.**

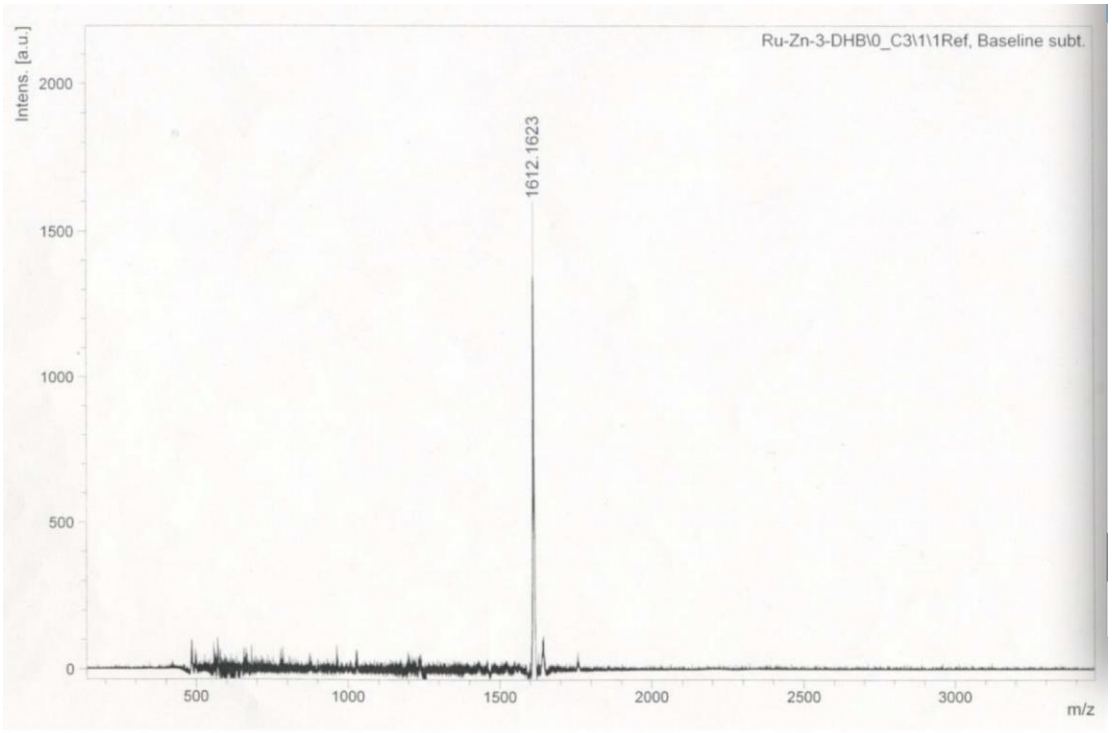

Figure S11. HR-MALDI-TOF Spectrum of conjugate **3.**

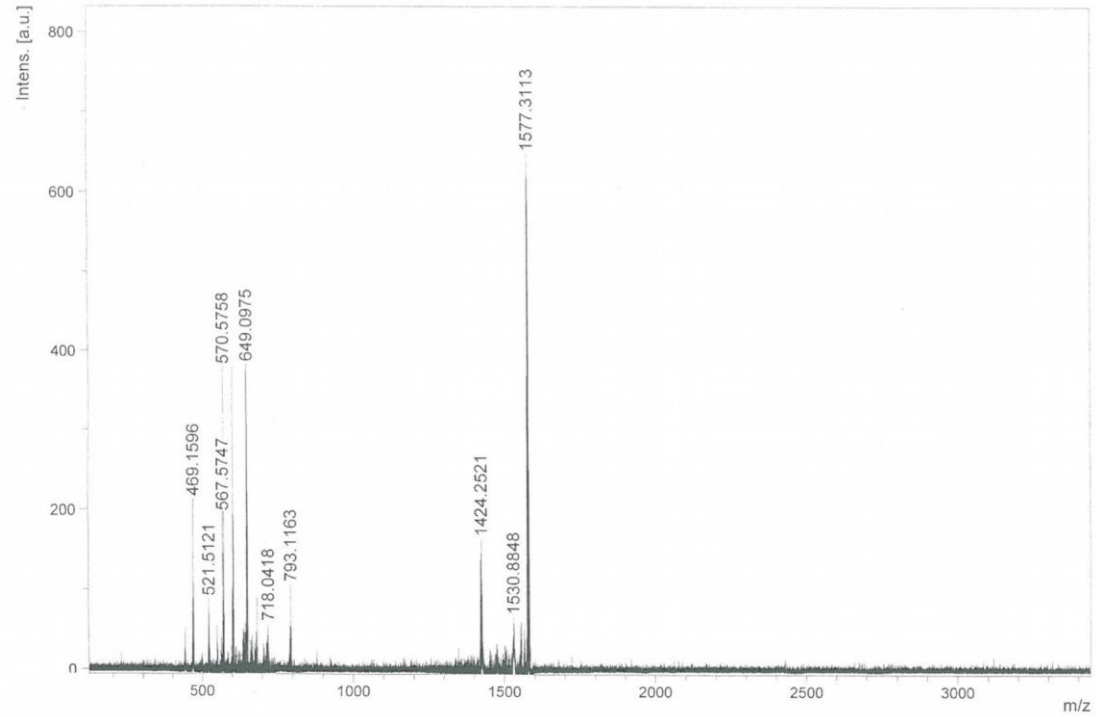

Figure S12. HR-MALDI-TOF Spectrum of conjugate **4.**

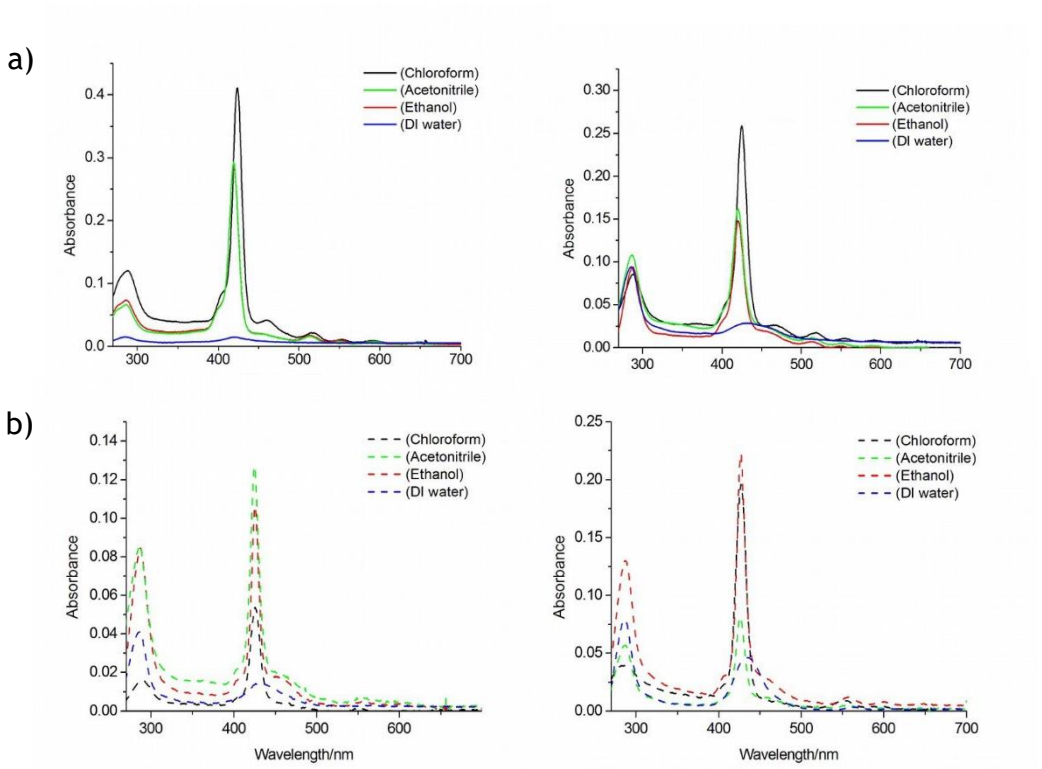

Figure S13. The absorption spectra of conjugates (a) **1** (left) and **2** (right), and (b) **3** (left) and **4** (right) in different solvents (chloroform, ethanol, acetonitrile and DI water). (1 μM, 298 K)

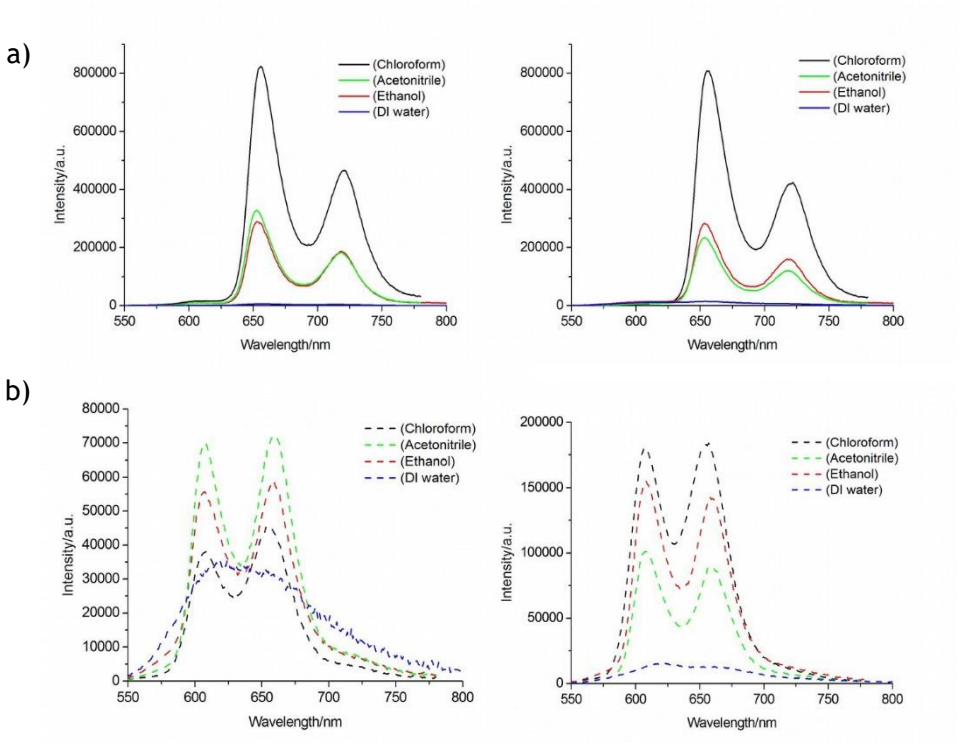

Figure S14. The emission spectra of conjugates (a) **1** (left) and **2** (right), and (b) **3** (left) and **4** (right) in different solvents (chloroform, ethanol, acetontrile and DIwater). (λ_{ex} = 430nm, 1 μM, 298 K)

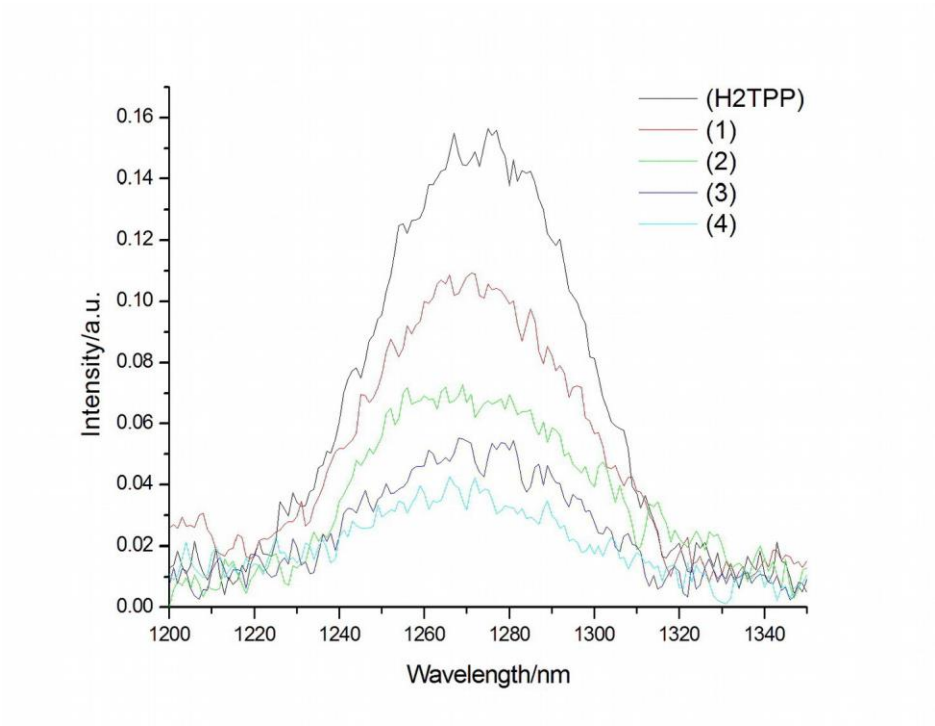

Figure S15. The near-infrared $^1O_2$ phosphorescence spectra (λ_{ex} = 420 nm) of conjugates **1-4** and the reference standard tetraphenylporphyrin, H_2TPP (in chloroform, Abs = 0.05).

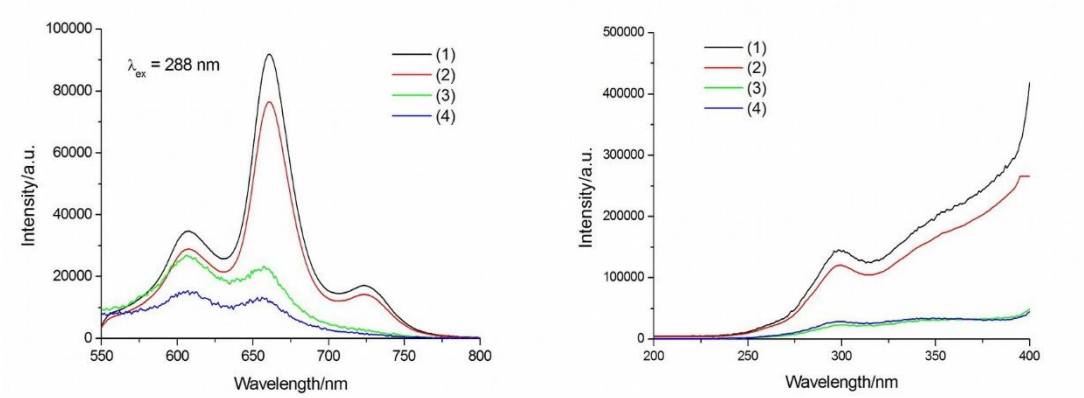

Figure S16. The emission spectra of conjugates **1**-**4** (left) in chloroform (λ_{ex} = 288 nm, 1 μM, 298 K); The excitation spectra of conjugates **1**–**4** (right) monitored at 661 nm in chloroform (1 μM, 298 K).

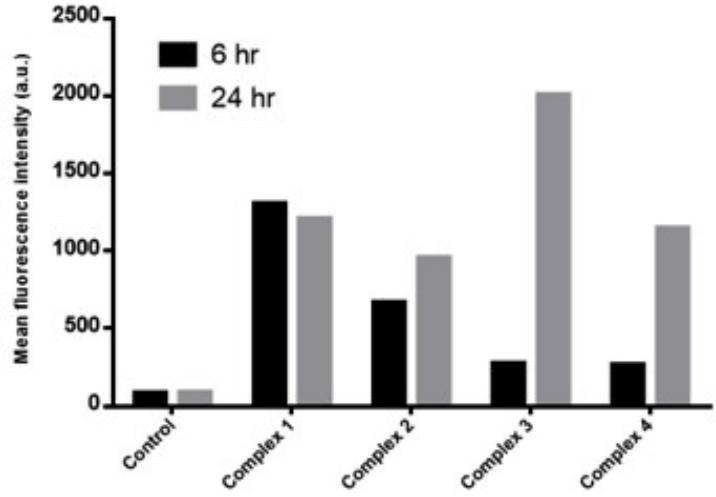

Figure S17. Flow cytometric analysis of cellular uptake of 10 μM of conjugates **1-4** by HeLa cells after incubation for 6 and 24 hr. Luminescence signal was excited by 633 nm and collected using a filter of 660/20 nm. At least 10000 events were counted. Measurements in the absence of complexes were prepared as control.

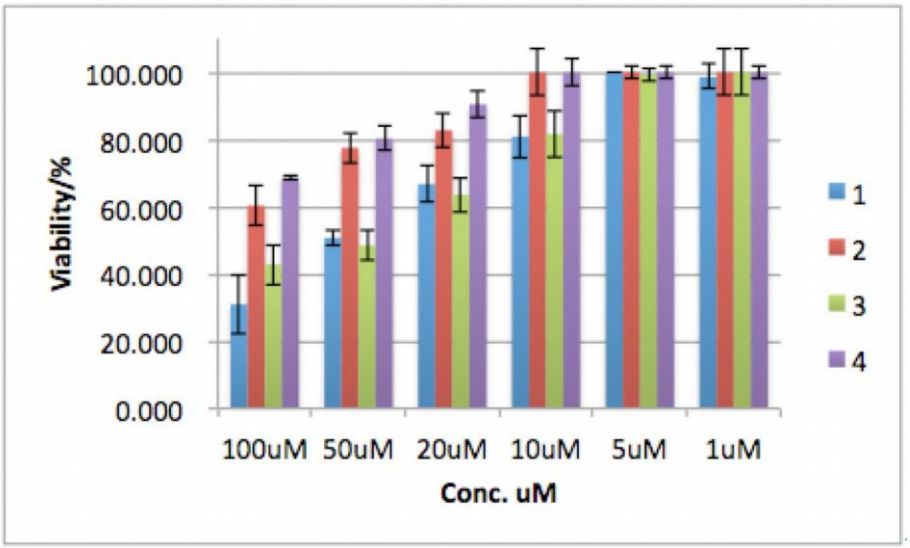

Figure S18. Dark cytotoxicity of free-base porphyrin-Ru(II) conjugates **1-4** were obtained using 1-100 μM of conjugates after incubation for 24 h in HeLa cells.

Table S1. The emission lifetimes of conjugates **1**–**4** in CH_3Cl, MeCN, EtOH and DI water. (λ_{ex} = 430 nm, λ_{em} = 600nm)

Compound	τ/ ns			
	$CHCl_3$	MeCN	EtOH	DI water
1	14.9	3.73, 26.9	5.19, 27.2	3.25, 12.1
2	17.3	3.22, 23.6	7.51, 30.8	3.61, 11.7
3	11.7	1.37, 22.7	2.01, 20.3	2.34, 50.37, 100.73
4	6.69	1.21, 17.7	2.56, 21.5	2.93, 29.6, 118.5

Excitation energy transfer in Ruthenium (II)-porphyrin conjugates led to enhanced emission quantum yield and $^1O_2$ generation

Jie Pan, Lijun Jiang, Chi-Fai Chan, Tik-Hung Tsoi, Kwok Keung, Shiu, Daniel W. J. Kwong,* Wing-Tak Wong,* Wai-Kwok Wong,* and Ka-Leung Wong*

Four amphiphilic ruthienium(II)-porphyirn complexes were prepared that display energy transfer conversion with zinc coordination, lysosome specific target, low dark toxicity and effecient photodynamic therapy.